Supporting Information

Vertically aligned MoS_2 Nanosheets on Monodisperse MXene as Electrolyte-Philic Cathode for Zinc Ion Battery with Enhanced Capacity

Wanting Su‡, Man Lang‡, Qingxiao Zhang, Yanan Yang, Weiwei Li, Huili Li* and Fang Zhang*

Key Laboratory of Resource Chemistry, Joint International Research Laboratory of Resource Chemistry, Ministry of Education, College of Chemistry and Materials Science, Shanghai Normal University, Shanghai 200234, China.

*E-mail addresses: li_huili@shnu.edu.cn; zhangfang@shnu.edu.cn.

‡Wanting Su and Man Lang contributed equally to this work.

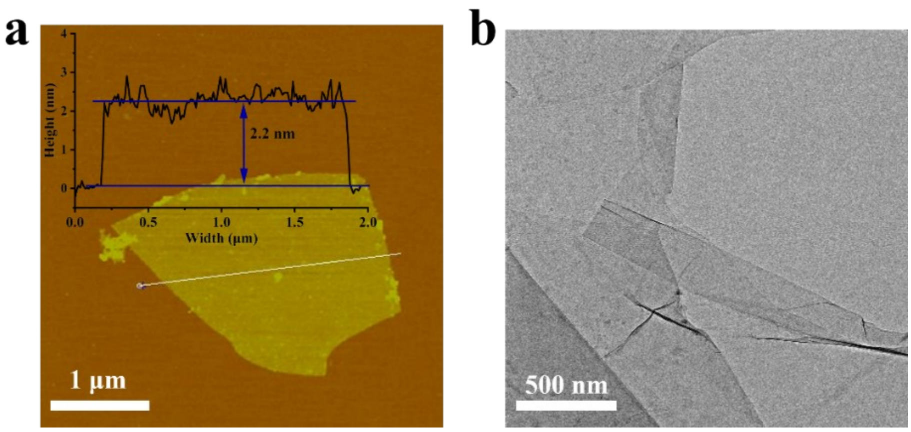

Figure S1. (a) AFM and (b) TEM images of $Ti_3C_2T_x$ MXene.

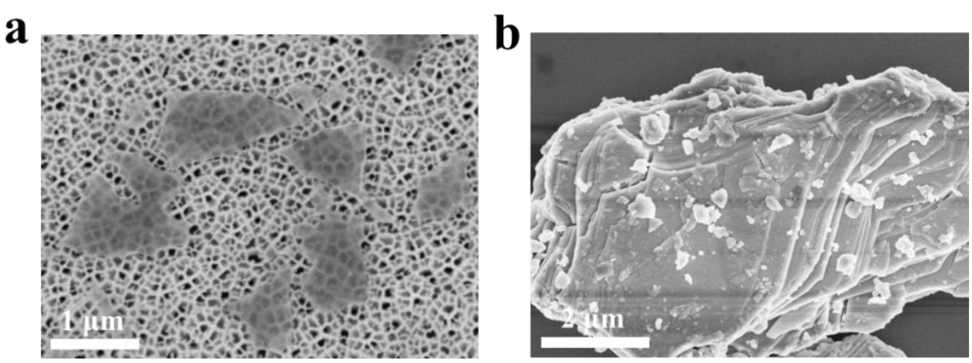

Figure S2. SEM images of (a) $Ti_3C_2T_x$ MXene and (b) Ti_3AlC_2 MAX.

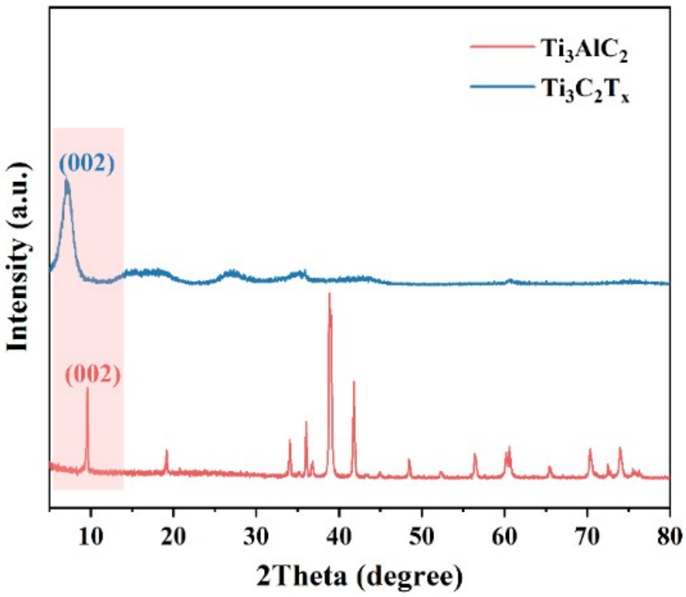

Figure S3. XRD patterns of Ti_3AlC_2 and $Ti_3C_2T_x$ MXene.

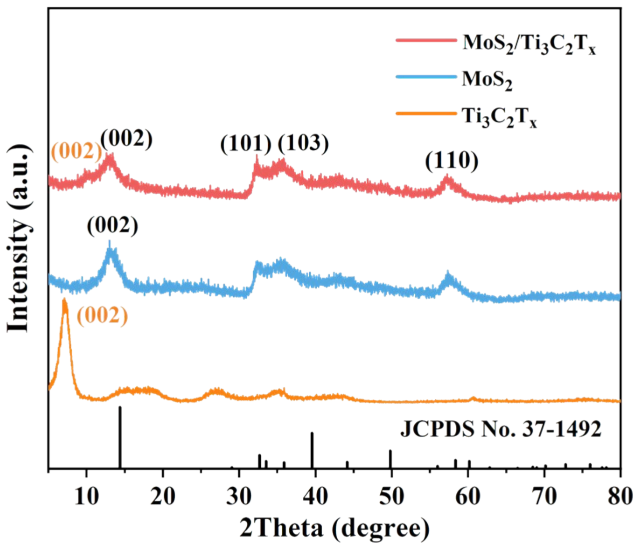

Figure S4. XRD patterns of MoS_2 and $MoS_2/Ti_3C_2T_x$ composites.

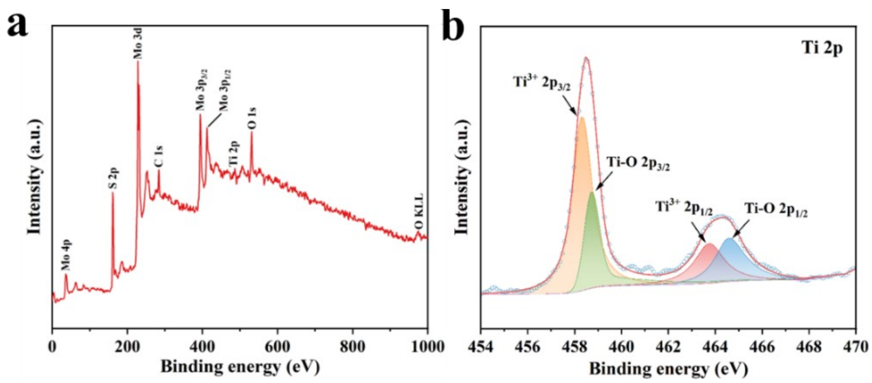

Figure S5. (a) XPS spectrum of $MoS_2/Ti_3C_2T_x$ MXene. (b) The high-resolution XPS spectrum of Ti 2p in the (a).

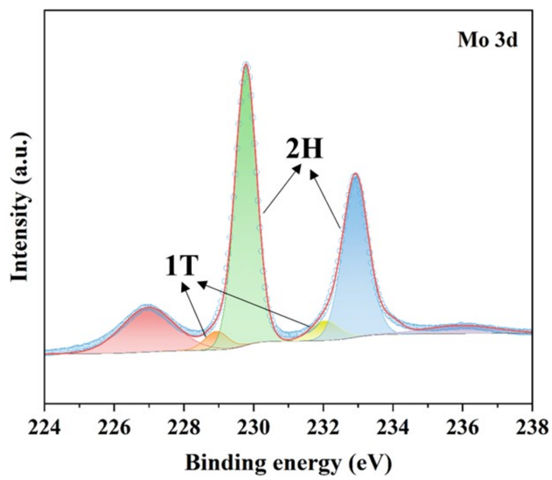

Figure S6. The high-resolution XPS spectrum of Mo 3d in the commercial MoS_2.

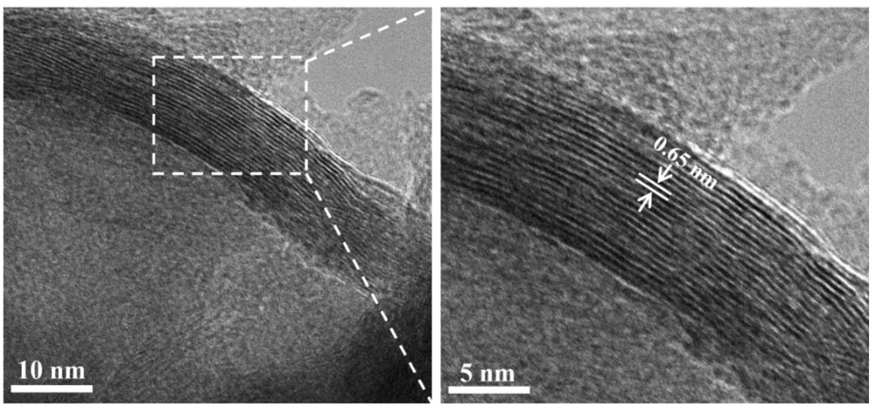

Figure S7. TEM images of MoS_2.

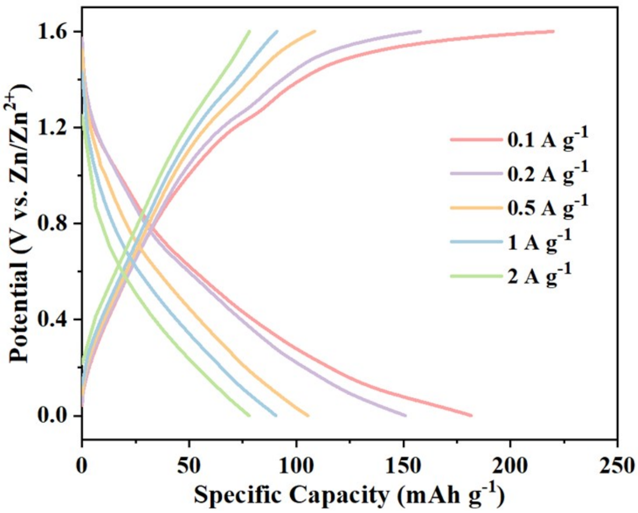

Figure S8. The galvanotactic charge/discharge curves of Zn//MoS_2 batteries under various current densities.

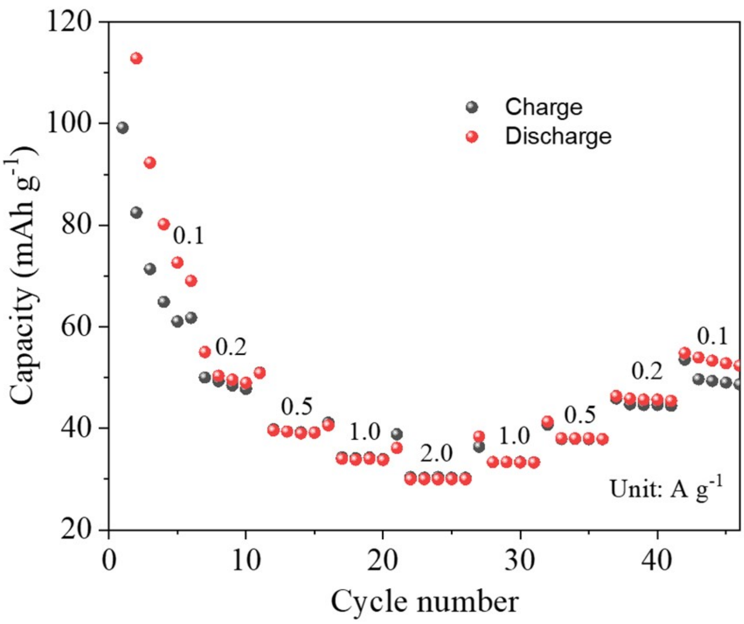

Figure S9. Rate capability of Zn//MoS_2/$Ti_3C_2T_x$ batteries with 1 mol L^{-1} $Zn(CF_3SO_3)_2$ electrolyte under various current densities.

Table S1. Discharge capacity of ZIBs compared with the values reported from other MoS_2 based ZIBs.

Cathode materials	Voltage window	Discharge capacity	Ref.
MoS_2-CC	0.25-1.25 V	198 mAh g^{-1} at 0.1 A g^{-1}, 180 mAh g^{-1} at 0.2 A g^{-1} 151 mAh g^{-1} at 0.5 A g^{-1}, 127 mAh g^{-1} at 1 A g^{-1} 100 mAh g^{-1} at 2 A g^{-1}	[1]
$MoS_2 \cdot nH_2O$	0.2-1.5 V	165 mAh g^{-1} at 0.1 A g^{-1}, 146 mAh g^{-1} at 0.2 A g^{-1} 122 mAh g^{-1} at 0.5 A g^{-1}, 100 mAh g^{-1} at 1 A g^{-1} 75 mAh g^{-1} at 2 A g^{-1}	[2]
MoS_2/CF	0.2-1.3 V	182 mAh g^{-1} at 0.1 A g^{-1}, 169 mAh g^{-1} at 0.2 A g^{-1} 149 mAh g^{-1} at 0.5 A g^{-1}, 131 mAh g^{-1} at 1 A g^{-1} 110 mAh g^{-1} at 2 A g^{-1}	[3]
MoS_2@CNTs	0.3-1.2 V	180.0 mAh g^{-1} at 0.1 A g^{-1}, 144.5 mAh g^{-1} at 0.2 A g^{-1} 126.7 mAh g^{-1} at 0.5 A g^{-1}, 112.8 mAh g^{-1} at 1 A g^{-1} 102.3 mAh g^{-1} at 2 A g^{-1}	[4]
MoS_2/PANI	0.2-1.3 V	181.6 mAh g^{-1} at 0.1 A g^{-1}, 152.1 mAh g^{-1} at 0.2 A g^{-1} 130.3 mAh g^{-1} at 0.5 A g^{-1}, 106.1 mAh g^{-1} at 1 A g^{-1} 83.2 mAh g^{-1} at 2 A g^{-1}	[5]
MoS_{2-x}	0.25-1.25 V	138.6 mAh g^{-1} at 0.1 A g^{-1}, 125.5 mAh g^{-1} at 0.2 A g^{-1} 112.8 mAh g^{-1} at 0.5 A g^{-1}, 95.6 mAh g^{-1} at 1 A g^{-1} 80.8 mAh g^{-1} at 2 A g^{-1}	[6]
MoS_2	0.25-1.25 V	168 mAh g^{-1} at 0.1 A g^{-1}, 151 mAh g^{-1} at 0.2 A g^{-1} 134 mAh g^{-1} at 0.5 A g^{-1}, 119 mAh g^{-1} at 1 A g^{-1} 104 mAh g^{-1} at 2 A g^{-1}	[7]
1T-MoS_2	0.25-1.25 V	164.1 mAh g^{-1} at 0.1 A g^{-1}, 149.5 mAh g^{-1} at 0.2 A g^{-1} 140.8 mAh g^{-1} at 0.5 A g^{-1}, 133.2 mAh g^{-1} at 1 A g^{-1} 120.1 mAh g^{-1} at 2 A g^{-1}	[8]
C-MoS_2-NC	0.2-1.4 V	249.7 mAh g^{-1} at 0.1 A g^{-1}, 219.9 mAh g^{-1} at 0.2 A g^{-1} 199.7 mAh g^{-1} at 0.5 A g^{-1}, 171.7 mAh g^{-1} at 1 A g^{-1} 152.8 mAh g^{-1} at 2 A g^{-1}	[9]
MoS_2-CTAB	0.2-1.3 V	197.9 mAh g^{-1} at 0.1 A g^{-1}, 179.3 mAh g^{-1} at 0.2 A g^{-1} 157.3 mAh g^{-1} at 0.5 A g^{-1}, 137.6 mAh g^{-1} at 1 A g^{-1} 118.8 mAh g^{-1} at 2 A g^{-1}	[10]
N-doped 1T-MoS_2	0.2-1.3 V	149.6 mAh g^{-1} at 0.1 A g^{-1}, 143 mAh g^{-1} at 0.2 A g^{-1} 133.1 mAh g^{-1} at 0.5 A g^{-1}, 124.4 mAh g^{-1} at 1 A g^{-1} 115.1 mAh g^{-1} at 2 A g^{-1}	[11]
MoS_2	0.3-1.3 V	191.2 mAh g^{-1} at 0.1 A g^{-1}, 177.4 mAh g^{-1} at 0.2 A g^{-1} 162.9 mAh g^{-1} at 0.5 A g^{-1}, 146.2 mAh g^{-1} at 1 A g^{-1} 129.6 mAh g^{-1} at 2 A g^{-1}	[12]
MoS_2-O	0.2-1.3 V	191.2 mAh g^{-1} at 0.1 A g^{-1}, 177.4 mAh g^{-1} at 0.2 A g^{-1} 162.9 mAh g^{-1} at 0.5 A g^{-1}, 146.2 mAh g^{-1} at 1 A g^{-1} 129.6 mAh g^{-1} at 2 A g^{-1}	[13]
Glu-MoS_2	0.3-1.5 V	182 mAh g^{-1} at 0.1 A g^{-1}, 121 mAh g^{-1} at 0.3 A g^{-1} 93 mAh g^{-1} at 0.5 A g^{-1}, 68 mAh g^{-1} at 0.8 A g^{-1} 52 mAh g^{-1} at 1 A g^{-1}	[14]
1T MoS_2/MWCNT	0.2-1.3 V	160.3 mAh g^{-1} at 0.1 A g^{-1}, 145.2 mAh g^{-1} at 0.3 A g^{-1} 129.3 mAh g^{-1} at 0.5 A g^{-1}, 107.4 mAh g^{-1} at 1 A g^{-1}	[15]
$MoS_2/Ti_3C_2T_x$	0-1.6 V	277 mAh g^{-1} at 0.1 A g^{-1}, 228 mAh g^{-1} at 0.2 A g^{-1} 176 mAh g^{-1} at 0.5 A g^{-1}, 139 mAh g^{-1} at 1 A g^{-1} 106 mAh g^{-1} at 2 A g^{-1}	This work

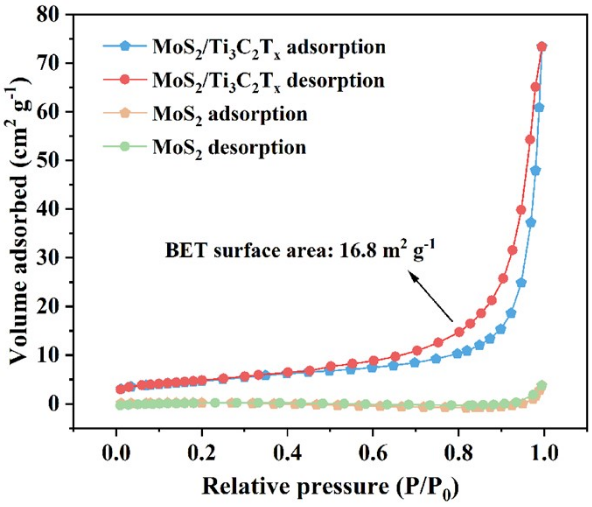

Figure S10. N_2 adsorption-desorption isotherm of MoS_2 and $MoS_2/Ti_3C_2T_x$ MXene composites.

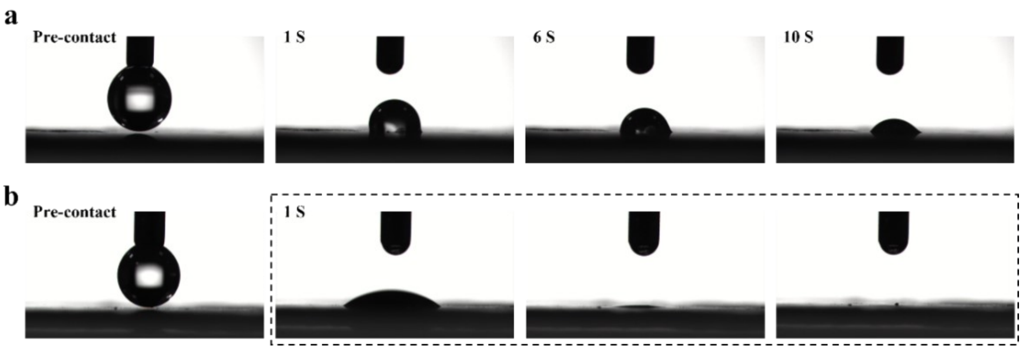

Figure S11. Water contact angles of a) MoS_2 and b) $MoS_2/Ti_3C_2T_x$ MXene composites.

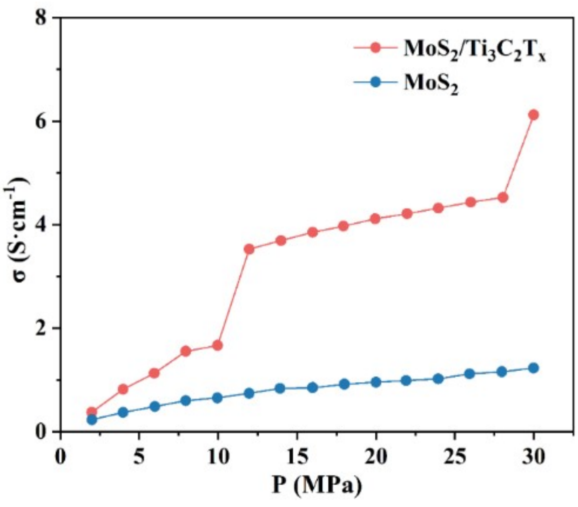

Figure S12. Electronic conductivity of $MoS_2/Ti_3C_2T_x$ composites and MoS_2.

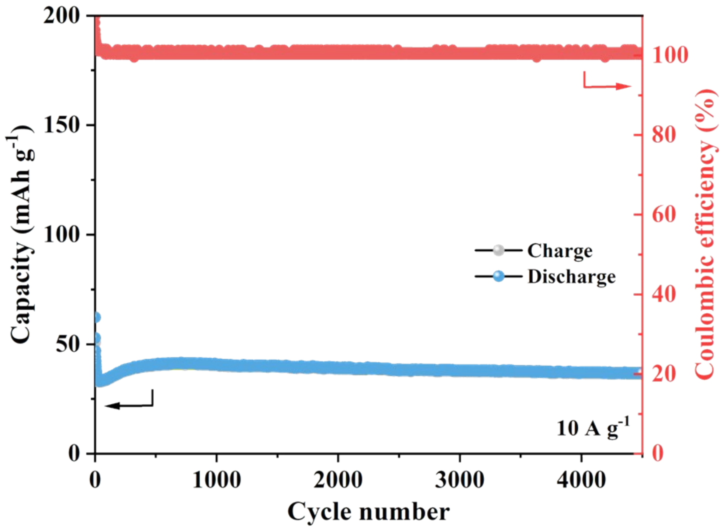

Figure S13. Long cycling performance of Zn//$MoS_2/Ti_3C_2T_x$ batteries at 10.0 A g^{-1}.

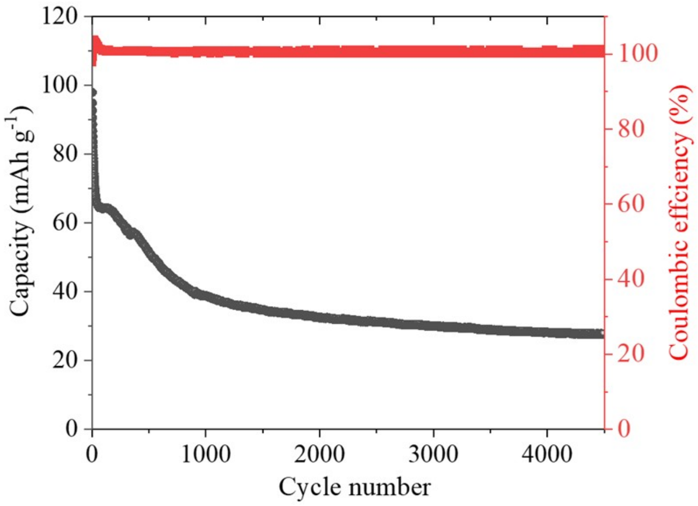

Figure S14. Long cycling performance of Zn//$MoS_2/Ti_3C_2T_x$ batteries with 1 mol L^{-1} $Zn(CF_3SO_3)_2$ electrolyte at 10.0 A g^{-1}.

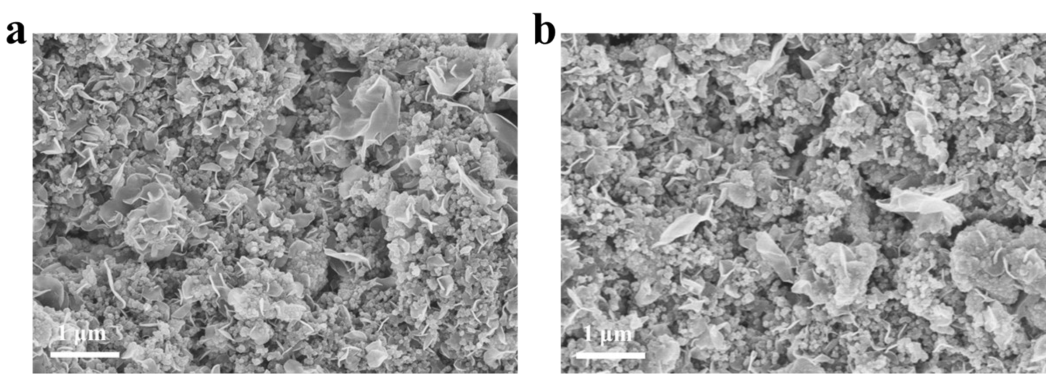

Figure S15. SEM images of the $MoS_2/Ti_3C_2T_x$ MXene electrode (a) before and (b) after cycles.

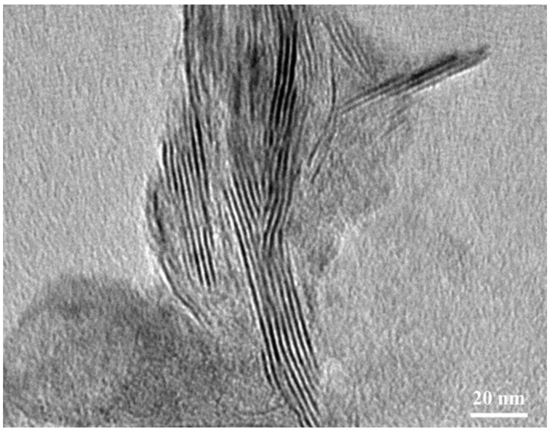

Figure S16. TEM image of the $MoS_2/Ti_3C_2T_x$ MXene electrode after cycles.

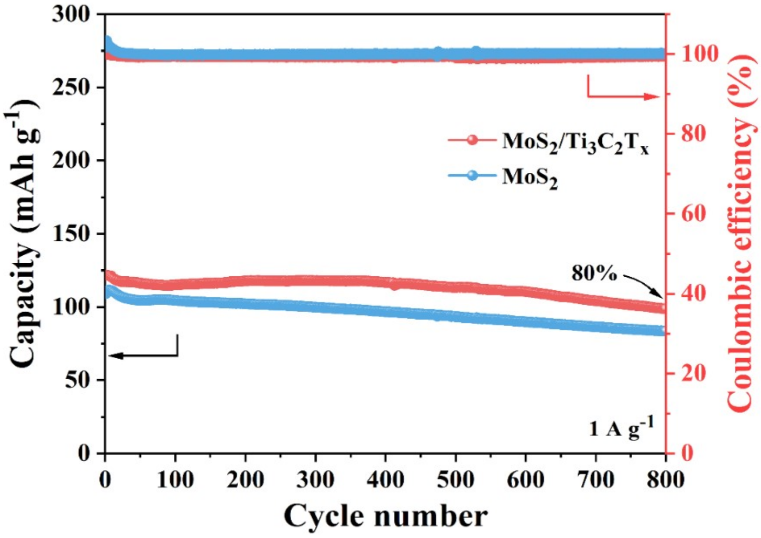

Figure S17. Long cycling performance of $Zn//MoS_2/Ti_3C_2T_x$ batteries at 1.0 A g^{-1}.

References

[1] J. Liu, N. Gong, W. Peng, Y. Li, F. Zhang, X. Fan, Vertically aligned 1 T phase MoS_2 nanosheet array for high-performance rechargeable aqueous Zn-ion batteries, Chem. Eng. J. 428 (2022) 130981.

[2] Z. Zhang, W. Li, R. Wang, H. Li, J. Yan, Q. Jin, P. Feng, K. Wang, K. Jiang, Crystal water assisting MoS_2 nanoflowers for reversible zinc storage, J. Alloy. Compd. 872 (2021) 159599.

[3] H. Liu, J.-G. Wang, W. Hua, Z. You, Z. Hou, J. Yang, C. Wei, F. Kang, Boosting zinc-ion intercalation in hydrated MoS_2 nanosheets toward substantially improved performance,

Energy Storage Mater. 35 (2021) 731-738.

[4] M. Huang, Y. Mai, L. Zhao, X. Liang, Z. Fang, X. Jie, Hierarchical MoS_2@CNTs hybrid as a long-life and high-rate cathode for aqueous rechargeable Zn-ion batteries, ChemElectroChem 7(20) (2020) 4218-4223.

[5] M. Huang, Y. Mai, L. Zhao, X. Liang, Z. Fang, X. Jie, Tuning the kinetics of zinc ion in MoS_2 by polyaniline intercalation, Electrochim. Acta 388 (2021) 138624.

[6] W. Xu, C. Sun, K. Zhao, X. Cheng, S. Rawal, Y. Xu, Y. Wang, Defect engineering activating (Boosting) zinc storage capacity of MoS_2, Energy Storage Mater. 16 (2019) 527-534.

[7] J. Liu, P. Xu, J. Liang, H. Liu, W. Peng, Y. Li, F. Zhang, X. Fan, Boosting aqueous zinc-ion storage in MoS_2 via controllable phase, Chem. Eng. J. 389 (2020) 124405.

[8] L. Liu, W. Yang, H. Chen, X. Chen, K. Zhang, Q. Zeng, S. Lei, J. Huang, S. Li, S. Peng, High Zinc-Ion Intercalation Reaction Activity of MoS_2 Cathode Based on Regulation of Thermodynamic Metastability and Interlayer Water, Electrochim. Acta, 410 (2022) 140016.

[9] C. Li, C. Liu, Y. Wang, Y. Lu, L. Zhu, T. Sun, Drastically-enlarged interlayer-spacing MoS_2 nanocages by inserted carbon motifs as high performance cathodes for aqueous zinc-ion batteries, Energy Storage Mater., 49 (2022) 144-152.

[10]. Cao, N. Chen, W. Tang, Y. Liu, Y. Xia, Z. Wu, F. Li, Y. Liu, A. Sun, Template-assisted hydrothermal synthesized hydrophilic spherical 1T-MoS_2 with excellent zinc storage performance, Journal of Alloys and Compounds, 898 (2022) 162854.

[11] Z. Sheng, P. Qi, Y. Lu, G. Liu, M. Chen, X. Gan, Y. Qin, K. Hao, Y. Tang, Nitrogen-Doped Metallic MoS_2 Derived from a Metal-Organic Framework for Aqueous Rechargeable Zinc-Ion Batteries, ACS Appl. Mater. Inter., 13 (2021) 34495-34506.

[12] M. Huang, Y. Mai, G. Fan, X. Liang, Z. Fang, X. Jie, Toward fast zinc-ion storage of MoS_2 by tunable pseudocapacitance, J. Alloys Compd., 871 (2021) 159541.

[13] H. Jia, M. Qiu, B. Tawiah, H. Liu, S. Fu, Interlayer-expanded MoS_2 hybrid nanospheres with superior zinc storage behavior, Compos. Commun., 27 (2021) 100841.

[14] Y.Q. Jin, H. Chen, L. Peng, Z. Chen, L. Cheng, J. Song, H. Zhang, J. Chen, F. Xie, Y. Jin, J. Shi, H. Meng, Interfacial polarization triggered by glutamate accelerates dehydration of

hydrated zinc ions for zinc-ion batteries, Chem. Eng. J., 416 (2021) 127704.

[15] Y.-T. Wang, Z.-Z. Zhang, M.-X. Li, One-Pot Synthesis of 1T MoS_2/MWCNT Hybrids for Enhanced Zinc-Ion Storage, Nano Futures, 6 (2022) 025001.